Carbon 189 (2022) 57–70

Contents lists available at ScienceDirect

Carbon

journal homepage: www.elsevier.com/locate/carbon

# Interaction of resorcinol-formaldehyde carbon aerogels with water: A comprehensive NMR study

Mónika Kéri [a, *], Dávid Nyul [a], Krisztina László [b], Levente Novák [a], István Bányai [a]

[a] University of Debrecen, Department of Physical Chemistry, H-4032, Debrecen, Egyetem tér 1, Hungary
[b] Budapest University of Technology and Economics, Department of Physical Chemistry and Materials Science, H-1521, Budapest, PO Box 91, Hungary

ARTICLE INFO

*Article history:*
Received 14 October 2021
Received in revised form
1 December 2021
Accepted 8 December 2021
Available online 9 December 2021

*Keywords:*
RF carbon aerogel
Pore morphology
Hydration mechanism
NMR cryoporometry
LF NMR relaxometry
Self-diffusion
Vapor adsorption

ABSTRACT

Carbon aerogels prepared from resorcinol-formaldehyde aerogels are promising platforms for electrodes, catalysts, adsorbents in environmental chemistry and as electric conductors. For these applications the knowledge of their structure and behavior in aqueous medium is essential. In this work two resorcinol-formaldehyde (RF) carbon aerogels prepared in different ways were characterized with various NMR methods while their pore structure was stepwise saturated with water. The wetting properties were studied by vapor adsorption and low-field NMR relaxometry, while the morphology was followed by NMR cryoporometry during the hydration process. At several water saturation levels the self-diffusion of water was measured. The comprehensive evaluation of the results led to a detailed description of the wetting process of these carbon aerogels beyond the pore size distributions. At low hydration level water clusters formed on and around the hydrophilic functional groups of the surface being able to adsorb water, but no continuous water layer developed on the surface. With increasing water content, spherical water drops formed inside the pore system, and vapor phase diffusion was observed in the partially filled pores. Subsequently the interconnected pore structure was saturated. The determined wet structure was compared to low temperature nitrogen gas adsorption results and scanning electron microscopy images.


## 1. Introduction

Porous materials are in the focus point of scientific research in the last decades due to their high specific surface area and wide application potentials. Carbon-based aerogels can be applied to various purposes like electrode materials, supercapacitors, adsorbents and even catalysts. Resorcinol-formaldehyde (RF) carbon aerogels prepared by pyrolysis from polymer precursor aerogels have high porosities and surface areas, adjustable pore structures, and other desirable properties like good electrical conductivity as well as thermal and mechanical characteristics, which make them promising candidates for the mentioned applications [1–9]. The pore size and the hydrophilic/hydrophobic character of the surface play important role, since the application is determined by the interaction between the solid material and the liquid (mainly aqueous) medium, the size and availability of the pores and the adsorption capacity as well [10].

The surface of carbon aerogels has basically a hydrophobic character, though the carbon skeleton is often decorated with heteroatom-containing functional groups. These are mostly oxygen functionalities, which form a primary binding site for water molecules, thus the oxygen content determines the degree of water filling and the level of hydrophilic character of the porous structure. Strong hydrophilicity can impede the adsorption of a non-polar adsorbate when carbon aerogels are used as adsorbents, but can be advantageous in other applications at the same time [10,11].

For these reasons the morphology and pore structure of carbon aerogels must always be highlighted. Nitrogen adsorption and desorption measurements, mercury porosimetry and microscopic techniques are applicable for size determination of micro- and mesopores [12], but none of them takes the potential structural changes and interaction in liquid medium into account; however, from the application point of view this information is essential. Water vapor adsorption [13] and nuclear magnetic resonance methods, namely low-field NMR relaxometry, diffusometry and cryoporometry, can be adaptable for this purpose [14–21]. Water vapor adsorption isotherms give information about the interaction

* Corresponding author.
*E-mail addresses:* keri.monika@science.unideb.hu (M. Kéri), nyul.david@science.unideb.hu (D. Nyul), laszlo.krisztina@vbk.bme.hu (K. László), novak.levente@science.unideb.hu (L. Novák), banyai.istvan@science.unideb.hu (I. Bányai).

https://doi.org/10.1016/j.carbon.2021.12.045

between water and the functional groups of the carbon surface. Relaxometry is able to distinguish water in different states inside the porous material (e.g., adsorbed or confined in pores), diffusometry depicts the mobility of water inside the pore system, while cryoporometry gives information about the shape and size of meso- and macropores. Together, they are able to reveal the wetting mechanism of porous materials [22]. The theoretical background of the applied NMR techniques is explained in details in the Supplementary Information.

These three NMR methods have recently been used for the structure exploration of different carbon-based materials, but mostly separately. Fairhurst et al. illustrated the applicability of $T_2$ relaxation measurements for the study of interfacial interactions and surface area of graphene oxide, nanographite and porous graphene [23]. Gogelashvili et al. studied water adsorption in active carbons by NMR relaxation, while Wang et al. measured $T_1$ relaxation time in activated carbons as a function of the vapor pressure, and described the mechanism of water cluster formation at the surface groups of the micro- and mesopores [24–26]. Their results showed good correlation with the models deduced from water adsorption isotherms [13].

Recently several complex NMR relaxation studies were published about the pore wettability of different RF xerogels and aerogels: Bardenhagen et al. applied water and DMSO as probe liquids, and found that the coupling between the pores of RF carbon xerogels depends on the quality of the solvent, hence the systematic saturation of the pores could unfold the wetting mechanism of these carbon materials [27]. Cadar et al. described a uniform surface layer of cyclohexane molecules while non-uniform distribution of water on carbon surfaces when they compared the wetting of carbon xerogels and aerogels with the two solvents [28,29]. These results were confirmed by the more restricted self-diffusion of the confined cyclohexane molecules [28]. Yu et al. described the restricted rotational motion and diffusion of adsorbed water molecules on carbon powders through low-temperature diffusion and relaxation experiments [30]. Liu et al. studied the water diffusion in carbon nanotubes and found quite fast restricted diffusion due to the weak interaction of water with the pore wall, and the ordered structure of confined water [31].

NMR cryoporometry and nitrogen adsorption methods often provide comparable pore size distribution curves, which indicates no significant structural change when dispersing the sample in liquid medium [32]. Recently, we also described that for RF aerogels the two techniques offer comparable results in the mesopore region, while perfectly complement each other with the micropore characterization on the part of gas adsorption and the macropore analysis on the part of cryoporometry [33]. We found that the pyrolysis of the polymer aerogel caused the shrinkage of wider pores, the appearance of cylindrical pores instead of spherical ones and the formation of a significant microporosity in the resulting carbon aerogel. Water freezing behavior and the state of water molecules was studied in carbon nanotubes by Ghosh et al. [34] Several NMR methods and gas adsorption results were compared in the study of activated carbons and carbon molecular sieves by Krutyeva et al. [35] In their paper the effect of different type of solvents and their interaction with the surface of the carbon samples were discussed in details. They characterized the pore structure with the combined use of nitrogen adsorption and NMR cryoporometry of samples completely saturated with organic liquids. The interactions between the surface and liquid were deduced from NMR relaxometry and diffusometry, which also helped to differentiate water in micro- and mesopores.

An ingenious direction of research can be the investigation of partially filled pore systems, since it can give deeper information about the interfacial interactions at low filling levels, while the stepwise saturation helps to understand the process of hydration. Relaxation of the liquid in the pores is strongly influenced by the interaction with the pore wall, thus from measuring the transverse relaxation times one can draw conclusion about the hydrophilic and hydrophobic character of the solid material and its wetting properties [27,28,36–38]. Pore size distribution curves of pores filled with various amount of liquid also show the pore-filling mechanism, namely whether the pores are gradually filled up or separately after each other. Allen et al. described the filling process of a silica with polar and non-polar liquids this way [39]. They carried out cryoporometry experiments at different filling levels and could characterize even the surface interactions accordant to their relaxometric results [36]. Diffusion of the liquid or even its vapor in partially filled pores also provides extra information about the studied systems. This phenomenon was widely studied by Ardelean et al. and D'Orazio et al. [40–43], and observed for carbon materials as well by Krutyeva et al. [35].

The aim of our study was to describe the morphology of two RF carbon aerogels in aqueous medium and to study in details the distribution of water during the wetting process. The saturation process was generated by gradual water addition to a given sample. We applied water vapor adsorption and the mentioned three NMR techniques to quantitatively describe the structure in aqueous medium and to build up a model for the hydration process. Results were compared to the dry structure determined with conventional methods like nitrogen gas adsorption and scanning electron microscopy (SEM). The detection windows of the applied methods and the comprehensive interpretation of their results are discussed as well.

## 2. Experimental

### 2.1. Synthesis and characterization of the carbon aerogels

Resorcinol-formaldehyde based carbon aerogels were obtained by sol-gel technique. For CA1 resorcinol (R, Merck) was dissolved in 3 mL water, then formaldehyde (F, 37% aq. solution, Merck) and $Na_2CO_3$ catalyst (C, Merck) were added. The concentration of R in the initial solution was 0.14 g/mL, R/F and R/C molar ratios were 0.5 and 50 respectively. The initial sol was sealed in glass vials and cured at 358 K for 7 days. The polymer precursor of the CA2 sample was synthesized in 3 mL water-1-ethyl-3-methylimidazolium ethyl sulphate (Sigma-Aldrich) mixture (43 V/V% water) under the same conditions but without $Na_2CO_3$, since the ionic liquid serves as a catalyst, as well as a porogen, i.e., a material which helps pore formation [7]. After solvent exchange the polymer lyogels were dried under supercritical conditions using carbon dioxide. The dry polymer aerogels were converted to carbon aerogels in a rotary quartz reactor under high purity dry nitrogen flow at 1073 K for 1 h.

Low temperature (77 K) nitrogen adsorption isotherms were measured by a NOVA 2000 (Quantachrome) automatic analyser. The apparent surface area $S_{BET}$ was calculated using the Brunauer–Emmett–Teller (BET) model [44]. A pore volume ($V_{0.98}$) was estimated from the amount of nitrogen adsorbed at relative pressure 0.98, assuming that the pores are then filled with liquid adsorbate. The micropore volume ($V_{micro}$) was derived from the Dubinin–Radushkevich (DR) plot [45]. The mesopore volume $V_{meso}$ was calculated as $V_{0.98}$ - $V_{micro}$. The pore size distribution was calculated with the quenched solid density functional theory (QSDFT) method using a carbon kernel for slit/cylindrical pores for the adsorption branch. The pore size distribution in the mesopore range was also calculated by the Barrett, Joyner and Halenda (BJH) model from both the adsorption and desorption branches of the isotherms [46]. (Strictly speaking the validity of this process is limited to the range 2–50 nm) Transformation of all the primary

adsorption data was performed by the Quantachrome software ASiQwin version 3.0. Water adsorption isotherms were measured gravimetrically by equilibrating *ca.* 150 mg carbon aerogel samples in an atmosphere of controlled relative humidity (RH) at 293.15 K.

### 2.2. NMR methods: experimental details and data evaluation

The carbon aerogel samples were powdered and kept at room temperature before the NMR measurements. Then water was added until over-saturation in several steps (from 0.1 g to 12.8 g water relative to 1 g of aerogel CA1 and to 1.4 g/g for CA2) at 298 K. It is important to note that the wetted solid carbon aerogels were powder-like, thus were easy to homogenize, and seized only at higher water contents. At each filling step $T_2$ relaxation time was measured, and at several water contents cryoporometry and diffusometry measurements were carried out.

Cryoporometric experiments were carried out on the 2.4, 4.85, 5.69 and 12.8 g/g samples for CA1 and 0.65, 1.4 g/g for CA2. The aerogels were put into plastic NMR tubes and weighted amounts of deionized (Milli-Q) water were added and equilibrated for one day. A 360 MHz Bruker Avance I. NMR spectrometer was used with a 5 mm direct QNP direct probe head, cooled with dried air by a BCU05 cooling unit. $^1$H spectra were recorded by a pre-optimized single time spin echo pulse sequence in order to reach the complete relaxation of the frozen liquid during the echo time (1 ms), and thus eliminate its broad signal from the spectrum [19,47,48]. The experiments started from the fully frozen state, and the melting and freezing processes were observed between 267 and 275 K, with 0.2–0.5 K steps. At every temperature, we waited 5 min for the equilibration after the nominal temperature stabilized. Ethylene glycol and methanol were used for calibrating the temperature sensor prior to the measurements and we also checked the melting point of the bulk water where it was observable [49]. MestReNova 9.0© was used for post-processing to obtain integrated intensity. Eq. S(1) was applied to calculate the pore radii from the melting and freezing point depressions. The $K_c$ of water was taken as 30 nm K, the shape of the pores was deduced from the melting-freezing hysteresis [19]. The integral-pore radius functions were fitted to asymmetric logistic curves (like the Richards and Gompertz growth functions) by OriginPro 8.6© software (e.g. Fig. S1) [50], and their analytical derivatives were applied to obtain the pore size distribution curves.

For low-field relaxation measurements, the carbon aerogel samples were introduced into 10 mm wide glass tubes, after mixing with water by hand and with ultrasonic bath as well, one day was allowed for equilibration. Water $T_2$ relaxation in the carbon aerogel samples was measured at 298 K with a 20 MHz Bruker the Minispec mq20 relaxometer using the standard CPMG pulse sequence [47,48]. We applied a pulse length of around 2 μs. Relaxation delays of 1–6 s was used, depending on the $T_1$ relaxation times. The echo time varied between 0.08 ms and 0.3 ms in successive CPMG experiments, and 500–1000 echoes were recorded to reach more than 90% decay of the signal intensity providing good basis for parameter estimation. The decrease of echo intensity as a function of time was fitted to the sum of exponentials on the one hand. On the other hand, the relaxation signal was converted into continuous distribution of relaxation components by inverse Laplace transformation [51,52]. The analysis was performed using the non-negative least square (NNLS) method making no preliminary assumptions about the number of the relaxation components. The MERA (*M*ulti-*E*xponential *R*elaxation *A*nalysis), a Matlab© based program was implemented for fitting [53]. Mostly 300 exponential terms were applied with a minimum curvature type of regularization and GCV (*G*eneralized *C*ross *V*alidation) as regularization parameter. This method provided a relaxation distribution with dominant relaxation times. We mostly had two relaxation domains and using bi-exponential least square fitting we had a good agreement for the characteristic $T_2$ values.

The self-diffusion of water molecules in the pore structure of the aerogels was measured with a stimulated spin echo pulse sequence using bipolar gradient pulses to decrease eddy currents (BIPLED) [54] on a Bruker Avance II 400 NMR spectrometer at 298 K. Diffusion time ($\Delta$) was 50 ms or 80 ms and the duration of gradient pulse ($\delta$) was 2 ms. In one experiment all parameters were kept constant except the pulse gradient strength ($G$), which was increased in 64 square distant steps in general, from 0 to ca. 33 Gauss cm$^{-1}$. The gradient was calibrated for $D_2O$ [55,56]. For post-processing the spectra MestReNova 9.0 software was used. Diffusion coefficients ($D_{obs,i}$) were calculated by fitting the measured echo intensity ($I$) as a function of $(\gamma^2\delta^2G^2(\Delta - \delta/3))$ according to Eq. S(7).

## 3. Results and discussions

### 3.1. Characterization of the carbon aerogels

The SEM images of the studied carbon aerogels (Fig. 1) show similar morphology. The interconnected microspheres of ca. 20 nm (Table 1.) form a pore network including also macropores.

Low temperature nitrogen adsorption isotherms were measured to reveal the micro- and mesoporous region. The isotherms are shown in Fig. 2a. The data deduced by the various models are summarized in Table 1. The nitrogen adsorption isotherms of the carbon aerogel samples are of Type IVa according to the latest IUPAC classification [57] implying the presence of micro- and mesopores beside the macropores, visible in the SEM images. Type H2b hysteresis loops indicate the interconnected pore network and pore blocking affected desorption [58].

The pore size distribution in the micro- and narrow mesopore range was best fitted supposing slit/cylindrical geometry (Fig. 2b). The DFT method shows a wide pore size distribution for both carbons in the 3–27 nm range, also implying the presence of wider mesopores. Like DFT, the BJH distribution from the adsorption branch confirms the larger mesopore volume of the CA1 sample (Fig. 2b and c). The size of the pore necks limiting the desorption process in both network systems can be deduced from the BJH distribution obtained from the desorption branch (Fig. 2d). The maximum for both carbons is around 20 nm, but while there is a window limited to 4–30 nm in the CA2 sample, it is much wider for the CA1 carbon. The higher micro- and mesoporosity of CA1 is reflected by all the derived data shown in Table 1.

Only carbon and oxygen atoms were detected by X-ray photoelectron spectroscopy (XPS), confirming that the ionic liquid is an "inert" porogenic solvent [7]. Although the surface of the carbon aerogels are intrinsically hydrophobic due to the carbon skeleton formed during the pyrolysis, XPS revealed the expected presence of oxygen containing functional groups on the surface, the O/C atomic ratio is 7.0% in both cases. Although no detailed analysis was performed on these samples, our previous studies on similar aerogels (O/C ratio of 5.5) found that the oxygen is present in single and double bonds with carbon atoms as *i)* C=O and in *ii)* R–OH or R–O–R [59]. These may serve as primary adsorption sites for water molecules in aqueous medium [11].

### 3.2. The interaction of the carbon aerogels with water

#### 3.2.1. Water vapor adsorption

The main source of information about the hydrophilic/hydrophobic nature of the carbon samples was provided by their water vapor adsorption isotherms. The adsorption branch of the water uptake isotherms is similar to that of Type V. The alike shape of the

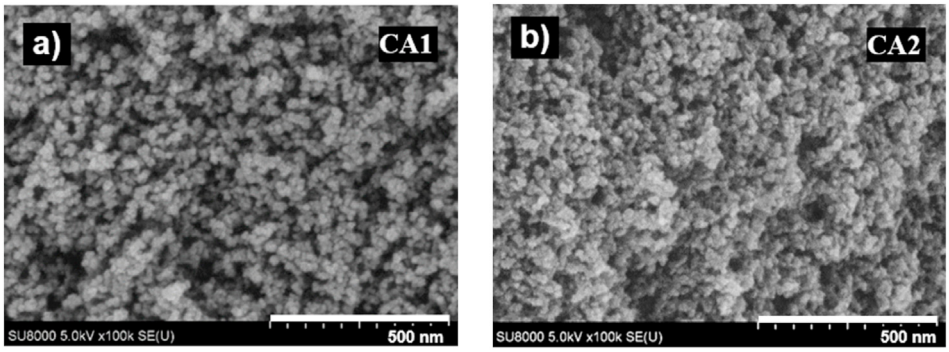


**Fig. 1.** SEM images of the carbon aerogels a) CA1 and b) CA2. The scalebars indicate 500 nm [7].

**Table 1**
Morphological properties of the carbon aerogels from nitrogen adsorption and SEM methods [7].

| Sample | $S_{BET}$ [a] | $V_{micro}$ [b] | $V_{tot}$ [c] | $V_{meso}$ [d] | $d_{SEM}$ [e] |
|---|---|---|---|---|---|
| | $m^2/g$ | $cm^3/g$ | $cm^3/g$ | $cm^3/g$ | nm |
| **CA1** | 865 | 0.35 (21%) | 1.66 | 1.31 | 20 ± 4 |
| **CA2** | 644 | 0.25 (23%) | 1.09 | 0.84 | 20 ± 3 |

[a] Surface area from BET model.
[b] Micropore volume.
[c] Pore volume at $p/p_0 = 0.98$.
[d] Mesopore volume ($V_{0.98}$ - $V_{micro}$).
[e] Diameter of the microspheres from SEM.

gravimetric water vapor adsorption isotherms (Fig. 3) confirms the identical surface O/C found from XPS, i.e., the hydrophobic/hydrophilic surface characteristics of the two carbons are very similar as far as the number of hydrophilic groups per gram is concerned.

The initial region of the isotherm (RH < 20%) is related to the hydrophilic character of the surface, which is governed by the primary active centres on the surface [60]. Both samples display a relatively sharp and similar increase in water uptake in the region 20–50%, where sorption in the micropores occurs. The water uptake estimated at the last point of the isotherm (RH = 95%) is 0.16 and 0.17 $cm^3/g$ for CA1 and CA2, respectively. These values are substantially smaller than the corresponding pore volumes

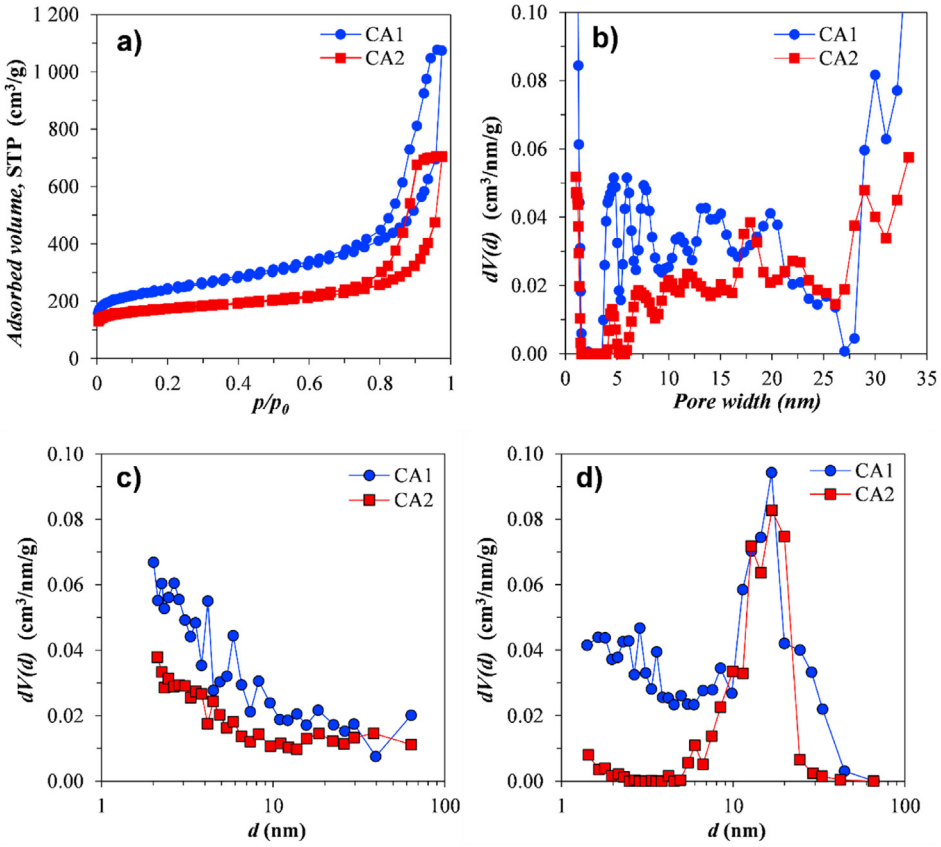


**Fig. 2.** a) Low temperature adsorption isotherms of carbon aerogel samples. b-d) Pore size distributions derived from the nitrogen adsorption isotherms. b) QSDFT, assuming slit/cylindrical pore geometry in the narrow pore range; c) BJH from the adsorption branch; d) BJH from the desorption branch sensitive for the pore necks' size. (A colour version of this figure can be viewed online.)

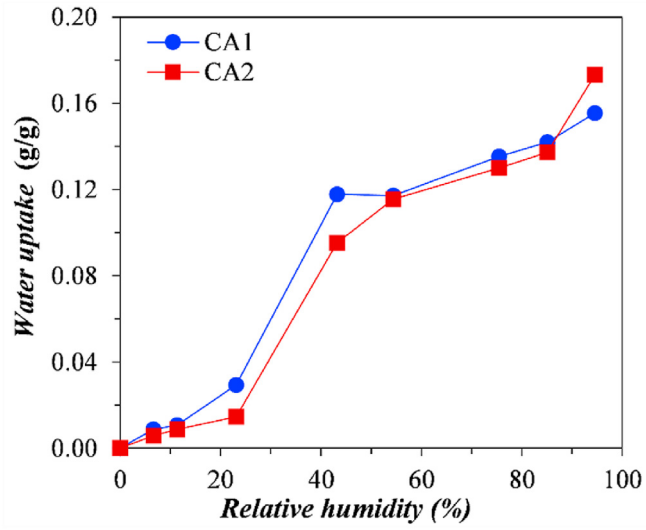


**Fig. 3.** Gravimetric water uptake of the carbon aerogels at 298 K. (A colour version of this figure can be viewed online.)

deduced from nitrogen adsorption measurements, i.e., in spite of their smaller size and higher kinetic mobility, the water molecules show a limited readiness to adsorb. It might be explained by the cluster-mediated pore filling mechanism of water during which pentameric ordered water molecular assemblies form in the carbon micropores independently on their hydrophobic or hydrophilic character both at lower and higher relative humidities [61]. Along the pore walls the adsorbed water exhibits long range order, while the "central layer", developing only in wider pores, is liquid like. Considering the higher surface area of CA1 (Table 1.) the same water uptake denotes lower density of hydrophilic functional groups on the surface of CA1, than on CA2. This is well presented above 40% relative humidity in Fig. S2., where the water uptake is related to the surface area.

It is important to note, that for the NMR measurements, the carbon aerogel samples were dried on air of a relative humidity around 50–60%. Thus, we suppose that the water molecules adsorbed on the hydrophilic groups and in micropores (ca. 0.12 g/g from Fig. 3) were present in the samples already at the beginning of the NMR measurements. Thus, water clusters rather than a single water layer have to be considered during the interpretation of NMR results.

### 3.2.2. Pore structure and morphology

In NMR cryoporometry experiments the melting and freezing properties of water in the pores of the carbon aerogels were followed at several water contents, up to the complete saturation of the samples, when meniscus appeared above the solid phase.

In the case of CA1, the $^1$H NMR spectrum of water at low added water contents (up to 2.4 g/g, where the cryoporometry experiment was carried out) showed two separated peaks at room temperature: (1) a low-intensity peak at ca. 0.5–1 ppm, which remained unchanged after freezing the sample, *i.e.*, the corresponding protons could not be frozen in the applied temperature range; (2) a high-intensity peak with a maximum around 6–7 ppm, which decreased in intensity during freezing, and started to increase during the melting process, thus it can be attributed to the pore-filling water (see Fig. 4). We assume that the low intensity peak at ca. 1 ppm belongs to the unfrozen water close to the surface of the solid material, which can be seen by cryoporometry as a residual peak in the frozen sample. This type of water belongs to water clusters formed around interfacial –O containing polar groups of the pore surface [11,62,63]. At higher water contents this small intensity peak could not be detected any longer; it may disappear by fusion with the pore-filling water or may be hidden under the broad, dominant peak. The $^1$H peak at low chemical shift value was observed for CA2 as well, but only at very low water contents (up to ca. 0.2 g/g), where no cryoporometry experiment was performed.

The melting and freezing curves of water in the carbon aerogels are shown in Fig. 5 a-c. The maximum NMR integral values of the water peak are normalized to the added water content of the samples. For CA1, at lower water contents (up to 5.7 g/g in Fig. 5a) the curves do not show any change at 273.1 K, only the adsorbed water clusters and pore-filling water is present in the sample. In the case of 2.40 g/g and 4.85 g/g filling levels, the melting and freezing processes occur in the same temperature range (ca. 268–270.5 K), only the amount of water belonging to these physical states increases. The most probable melting and freezing point of water (the highest slope of the melting and freezing curves) in these pores is ca. 270.2 K and 269 K respectively (see Fig. 5a, solid lines). As compared to the bulk transition temperature the ratio of the freezing and melting point depressions is close to 3/2 ($\Delta T_f/\Delta T_m \approx 1.7$) indicating sphere-like water-filled pores in CA1 (details are in the SI) [19].

The size distribution of the pores ($r_p$) can be calculated from the melting- and freezing point depressions ($\Delta T_{m/f}$) according to Eq. S(1). Considering spherical geometry, the pore radius can be derived from the melting point depression with Eq. (1).

$$\Delta T_m = T_m - T_0 = -\frac{2K_c}{r_p} \quad (1)$$

where $T_m$ is the melting point of the liquid in the porous system, $T_0$ is the transition temperature of the bulk liquid, $K_c$ is the cryoporometric constant of water, while $r_p$ is the radius of the pore [19]. The pore diameter is about 42 nm from Eq. (1)., and the calculated pore size distributions are shown in Fig. 5d (blue color). There are small deviations (±1 nm) between the most probable values of size depending on the water content or calculation from either the freezing or the melting processes (Fig. 5d, Fig. S4.).

Cryoporometry results give information about the filling mechanism of the pores as well [39]. In CA1, at the lowest measured filling state (2.4 g/g) only the 42 nm pores are observable. The increasing amount of water in the sample fills more and more pores of this size, since the determined pore size does not change. At about 4.8 g/g these pores get saturated. At higher filling state (until 12.8 g/g, Fig. 5b) these pores remain saturated (~4.8 g/g, lower dashed line), but the melting and freezing curves get closer to each other. We explain this narrowing hysteresis with the fusion of the saturated pores, which modifies the strict spherical geometry [18,21].

From 5.69 g/g water content a second melting/freezing step appears between 271 and 272 K, showing no hysteresis (Fig. 5a). Further filling (12.8 g/g) results in the saturation of these larger pores up to 10.75 g/g (Fig. 5b, upper dashed line). Due to the lack of hysteresis, the pore size cannot be unequivocally derived from the curves. In our assumption these pores form an interconnected pore network and join the saturated spherical pores. At 12.8 g/g water content, the sample is oversaturated, liquid phase is visible above the sample, and water appears with melting point around 273 K.

For CA1 the often-used incipient wetting value, meaning the water content where the carbon surface gets shiny during the saturation process, is 5.4 g/g, similarly to the saturation of the spherical pores (4.80 g/g). Cryoporometry showed that even 10.75 g/g water can be introduced to the pore structure without

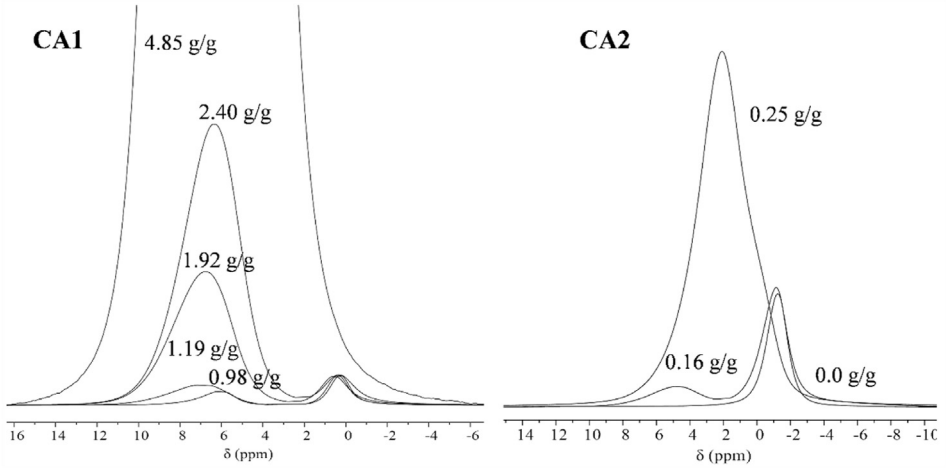


**Fig. 4.** High-resolution $^{1}$H NMR spectra of water in carbon aerogel CA1 and CA2 at low water contents. The intensities of the spectra are normalized to the peak at about 0 ppm.

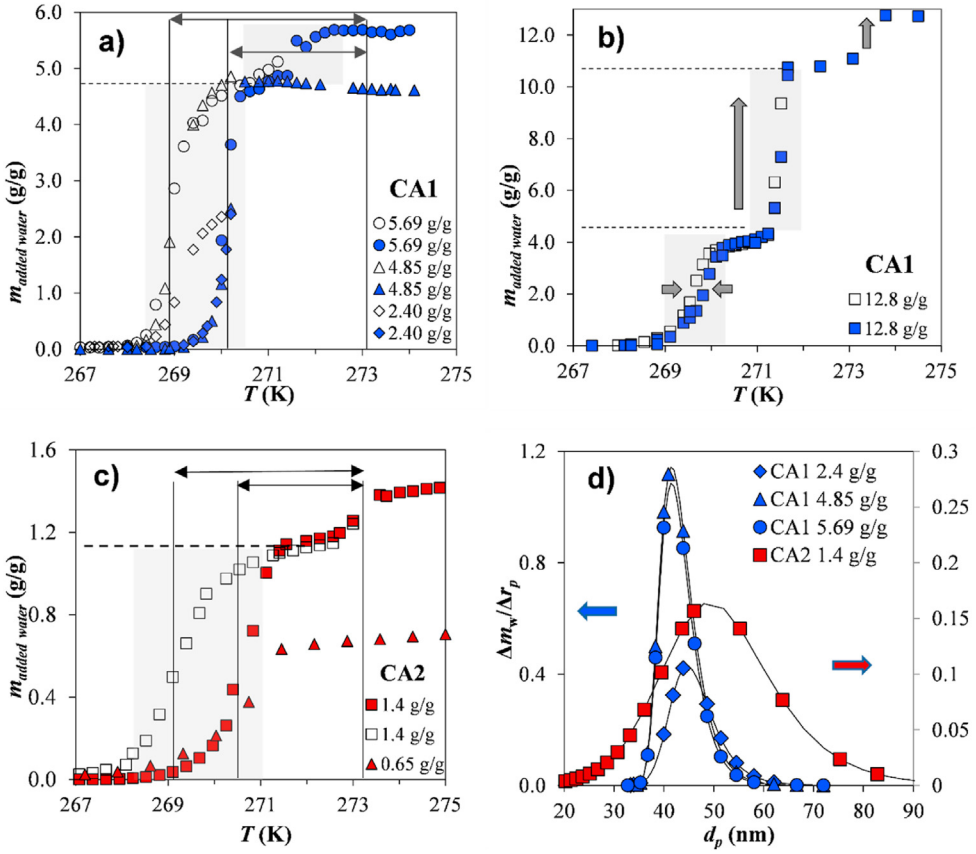


**Fig. 5.** a-c) Melting and freezing curves: a) CA1, 2.4–5.69 g/g filling level; b) CA1, 12.8 g/g filling level, where arrows denote the observed shifts; c) CA2, 0.65–1.4 g/g filling level. Empty and filled symbols stand for the freezing and melting processes respectively. Grey rectangles highlight the phase transitions belonging to each pore type. Solid lines indicate the melting and freezing temperatures, double arrows show the melting and freezing point depressions, while dashed lines show their saturation levels. d) The pore size distribution of CA1 and CA2 at several filling states, derived from the melting curves. Symbols show measured data, lines are calculated from fitting with logistic curves. (A colour version of this figure can be viewed online.)

changing the texture of CA1, thus the pore-filling water amount can be estimated in a more exact way.

For CA2, NMR cryoporometry was measured at a partially filled state (0.65 g/g water content), and above the saturation (1.4 g/g). In the partially filled sample a melting process is shown with a ca. 2.6 K melting point depression (in Fig. 5c, solid lines and double arrow), and no bulk water is present. In the saturated sample bulk water appears as a step at 273.1 K, and a well-defined freezing-melting hysteresis can be detected (Fig. 5c). For the two filling states, the melting processes partially overlap with each other from 269 to 271 K, indicating the same type and size of pores. In the saturated sample, the temperature range of the hysteresis, the

inflexion points (indicated with solid lines in Fig. 5c), and thus the $\Delta T_f/\Delta T_m$ ratio ($\approx$1.7) is similar to the case of CA1 (Fig. 5a), but for CA2 the curves are less steep. This leads to the conclusion that the pores in CA2 have spherical geometry as well, approximately the same pore size (ca. 50 nm), but a wider pore size distribution than in CA1 (Fig. 5d). These pores in CA2 are filled completely with about 1.16 g/g water amount only (Fig. 5c, dashed line), unlike the 4.8 g/g pore water content of CA1. This difference is reflected in the maximum height of the pore size distribution curves in Fig. 5d. For CA2 no other melting-freezing step was detected, which means that the size of these connecting pores may be above the detection limit of the cryoporometry technique (detailed in the SI).

The SEM images of the aerogels (Fig. 1) and our previous paper [33] as well confirm the assumption that the space between the aerogel beads can be approximated with spheres, i.e. the spherical pores indicate water drops surrounded by the aerogel network. This may result either from the higher density of hydrophilic −O containing functional groups in these points of the structure or from the lower Laplace-pressure therein. The interconnected pore network, observed in CA1, is formed between the aggregated aerogel beads. The pore size distribution curves of the carbon aerogel derived from NMR cryoporometry (Fig. 5d) and $N_2$ adsorption (Fig. 2b–d) complete well each other. DFT shows a wide distribution of mesopores but from 30 nm the curves increase, indicating larger mesopores beyond the detected size range. These larger meso- and macropores were detected more precisely by NMR cryoporometry.

Supposing spherical pore geometry, the pore radii, and the water volume filling these pores (4.80 $cm^3/g$ and 1.16 $cm^3/g$ for CA1 and CA2, respectively, see Fig. 5a and c) the specific surface area ($S_{cryo}$) of these spherical pores can be estimated (the detailed calculations can be found in the SI, while the results are shown in Table 2). Surface areas of 686 $m^2/g$ for CA1 and 139 $m^2/g$ for CA2 are calculated, reflecting the difference of the aerogels in the hydrated state. These surface area data are somewhat different from the specific surface determined from $N_2$ gas adsorption (865 $m^2/g$, and 644 $m^2/g$ for CA1 and CA2 respectively, Table 1), which highlights the different pore size limits of the methods and unlike behavior of the pore-filling materials.

As a preliminary conclusion, NMR cryoporometry revealed spherical pores with similar size ($d$ = 40–50 nm) in both wet carbon aerogels. However, there was a significant difference in the pore volume, *i.e.,* the amount of water in the saturated spherical pores (4.80 g/g and 1.16 g/g for CA1 and CA2 respectively), which confirms the looser structure of CA1. The saturation of the mesopores with water follows the similar mechanism:

- Adsorbed water clusters are present and detected in the $^1$H NMR spectra.
- During the water uptake spherical like water droplets appear one after another, as the basically hydrophobic material does not allow homogeneous water distribution.
- Water fills up the connecting pore system, whose size is in the meso- and macropore range and can be detected by NMR cryoporometry in CA1, but may exceed the detection window of the technique and thus not observed in CA2.

**Table 2**
Properties of the carbon aerogels saturated with water from NMR data.

| Sample | $d_{pore}$ [a] | $m_{pore\ water}$ [b] | $S_{cryo}$ [c] | $l$ [d] | $\xi$ [e] |
|---|---|---|---|---|---|
| | nm | g/g | $m^2/g$ | nm | m/s |
| **CA1** | 42 | 4.80 | 686 | 0.22 (±0.007) | $4.17\times10^{-8}$ ($\pm1.3\times10^{-9}$) |
| **CA2** | 50 | 1.16 | 139 | 0.19 (±0.013) | $1.15\times10^{-7}$ ($\pm7.8\times10^{-9}$) |

[a] Diameter of the spherical mesopores from NMR cryoporometry.
[b] Water in saturated spherical mesopores.
[c] Surface area of the spherical mesopores from cryoporometry.
[d] The thickness of surface water layer from relaxometry.
[e] Surface relaxation strength from relaxometry.

### 3.2.3. Hydration properties and pore size by relaxometry

Low-field relaxometry provided a further opportunity to characterize the hydration properties and mechanism of the studied carbon aerogels at several filling states. The two sites relaxation model was applied, which differentiates two types of liquid, surface liquid (under the influence of the pore surface, covered by bulk liquid) and bulk liquid. Provided fast molecular exchange exists between these liquids, the measured transverse relaxation rate constant ($1/T_2$) can be expressed by the weighted average of the relaxation rate of the liquid in the bulk-like ($1/T_{2bulk}$) and the surface region ($1/T_{2s}$) (Eq. (2).):

$$\frac{1}{T_2} = \frac{V_s}{V}\frac{1}{T_{2s}} + \frac{V_{bulk}}{V}\frac{1}{T_{2bulk}} \quad (2)$$

where $V$ is the total volume of the liquid measurable by relaxometry, $V_s$ and $V_{bulk}$ are the volumes of the surface liquid and the bulk liquid respectively. $T_2$ is the measured average transverse relaxation time, while $T_{2bulk}$ and $T_{2s}$ are the characteristic relaxation time constants of liquid molecules in the bulk-like and surface region respectively [36]. The measured decays of transverse magnetization in time, obtained from CPMG experiments, have shown one or two exponential components depending on the sample and its actual water content. Accordingly, we applied mono- or biexponential least square fitting to the decay curves, and the number of the exponentials was confirmed additionally by the inverse Laplace transformation method (see an example in Fig. S5 and in Fig. 7c).

The determined most probable $T_2$ values are presented in Fig. 6a and b as a function of the added water content. The two $T_2$ values ($T_{2a}$ and $T_{2b}$) can be attributed to water being present in two compartments with different relaxation rates. As the amplitudes of the fitted exponentials are proportional to the number of protons relaxing at the same rate, we calculated the amount of water in both compartments ($m_i$) from the total amount of added water ($m_{added\ water}$) and plotted it as a function of the added water content (Fig. 6c for CA1 and Fig. 6d for CA2). This interpretation is based on the model according to Eq. (2).

For CA1 below about 0.5 g/g water only one relaxation process can be observed with increasing transverse relaxation time constant (Fig. 6a, $T_{2a}$ with half empty symbols) and amplitude (Fig. 6c, $T_{2a}$) by increasing water content. In the air-dried sample (no added water) 5.3 ms $T_2$ relaxation time was measured, indicating the presence of water clusters. The immediate growth of $T_2$ can be attributed to the increasing number of water layers around these clusters, thereby forming larger ones. We suppose that these sites are around the above-mentioned oxygen containing groups of the aerogels, behaving as hydrophilic spots on the carbon skeleton [11]. Between ca. 0.5 and 2.0 g/g water content the $T_{2a}$ and its mass ratio is constant, indicating the parallel formation of water clusters, and their fusion into the pore-filling water appearing as $T_{2b}$ (Fig. 6a and c). Above $m_w \approx$ 2 g/g the amount of water ($m_i$) in the clusters gets decreasing, as the clusters are incorporated into the pore-water and cannot be detected above 4 g/g saturation. At 0.9 g/g water content a component of longer $T_2$ appears ($T_{2b}$), indicating the appearance of water molecules which are less affected by those having restricted motion near the surface. In our explanation, from this point water gradually fills out pores of the structure one at a time, resulting in very slightly increasing $T_2$ (from about 120 to 160 ms) and steeply linearly increasing $m_i$ (see Fig. 6c).

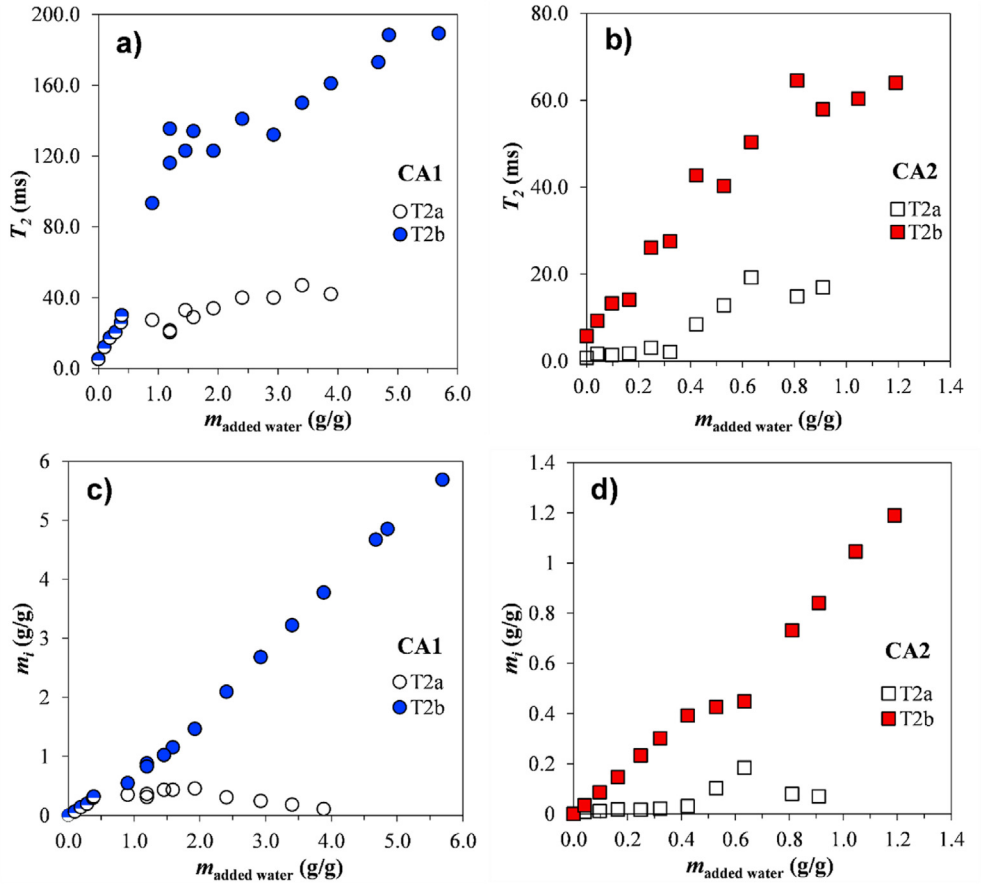


**Fig. 6.** a-b) Transverse relaxation times of fast-relaxing ($T_{2a}$) and slow-relaxing ($T_{2b}$) water and c-d) the amount of water in each compartment ($m_i$) for CA1 and CA2 as a function of the water content. (A colour version of this figure can be viewed online.)

The wetting mechanism of CA2 differs somewhat from that of CA1. A significant contrast is that two relaxation domains are observed from the first addition of water. Here $T_{2a}$ has a constant low value (0.7–3 ms) up to 0.4 g/g water content indicating multilayered water clusters near the surface with constant amount (Fig. 6b and d). This suggests that CA2 has more hydrophilic functional groups on the carbon skeleton, which is already hydrated at ambient humidity. The constant water amount in these clusters may be the consequence of two processes; *i)* continuous transformation to larger pore-filling water drops (red squares in Fig. 6b) and parallel formation of new clusters; *ii)* the number of water clusters remains constant and the pore-filling starts at different sites. The $T_2$ value and the water content of this domain increases from 0.4 g/g showing the appearance of extra water layers on the clusters. In parallel, there is another type of water molecules with higher $T_2$ relaxation time ($T_{2b}$) which value monotonously increases during the saturation process and reaches a $T_2$ value around 60 ms above ~ 0.7 g/g water content. We ascribe this relaxation domain to the water filling the mesopores, also confirmed by the cryoporometry results (Fig. 5c).

We have to note that the measured $T_2$ relaxation times are significantly lower for CA2 than that for CA1 (see Fig. 6a and b). Since cryoporometry and $N_2$ adsorption confirmed that the pore size distribution of the two carbon aerogels is similar for the mesopores, the generally lower $T_2$ values of CA2 are not caused by the different confinement of the water molecules, but indicates higher relaxivity effect of the surface.

In partially saturated porous media, the wetting and saturation process can be followed by the transverse relaxation time constant of the fluid at different filling states. For the studied carbon aerogels cryoporometry has unequivocally proved the presence of spherical pores filled with water at several stages of the wetting. The filling process of these pores completed at ca. 4.8 g/g for CA1 and at 1.16 g/g for CA2 (see dashed lines in Fig. 5a–c), thus for this regime of wetting, we could calculate the filling degrees, $f$ as a function of water content. The filling degree is the ratio of the actual water content of the pores (Fig. 6c and d, belonging to $T_{2b}$) and the water content of the completely filled pores, i.e., 4.8 g/g and 1.16 g/g ($V_{pore}$). Its relationship with the transverse relaxation rate gives information even about the wettability of the surface and the saturation mechanism of the pores through an empiric coefficient, $k$ (Eq. (3).) introduced by Ardelean [38].

$$\frac{1}{T_2} = \xi \frac{S_p}{V_p} \frac{1}{f^k} + \frac{1}{T_{2bulk}} \tag{3}$$

Here $S_p$ is the specific surface area, $V_p$ is the total volume of the given pores in 1 g of solid. $\xi$ is the surface relaxation strength, an empirical physical constant for the solid-liquid interface in the system, which is

$$\xi = l\left(\frac{1}{T_{2s}} - \frac{1}{T_{2bulk}}\right) \tag{4}$$

where $T_{2s}$ is the surface relaxation time constant and $l$ is the liquid layer thickness on the surface in interaction with the bulk water. Gallego-Gomez et al. obtained a simpler formula for the relation

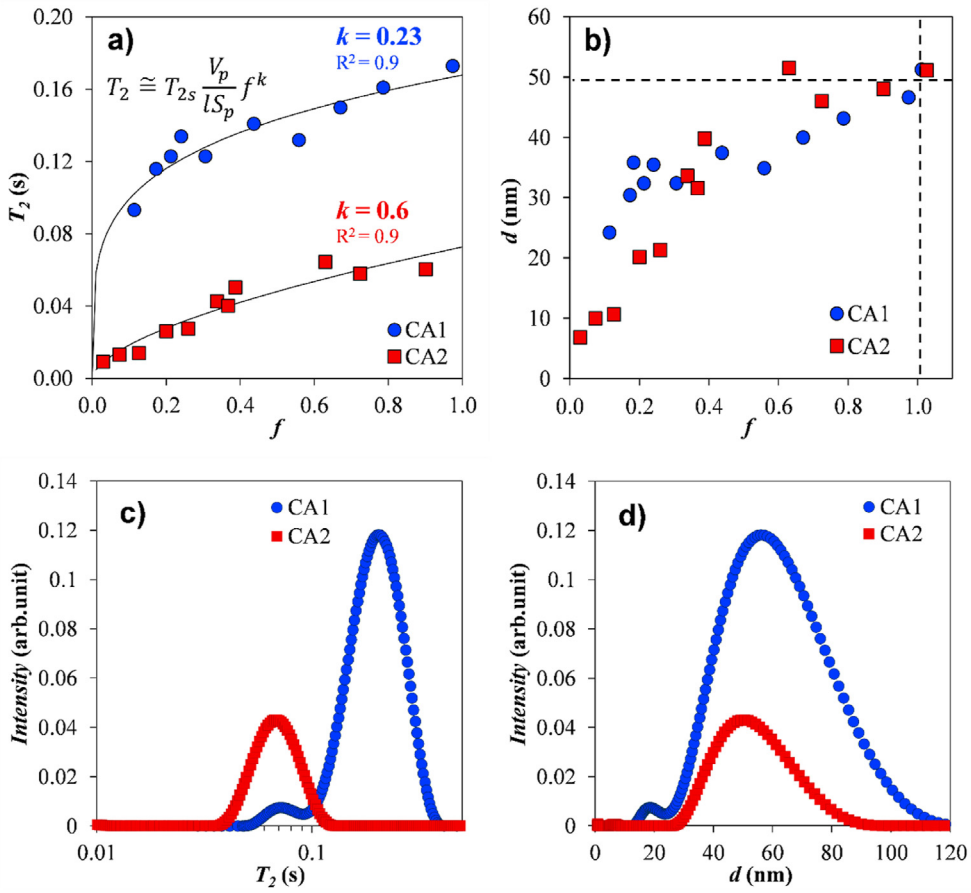


**Fig. 7.** a) Transverse ($T_2$) relaxation time constants as a function of the filling factor in RF carbon aerogels fitted with Eq. (5), and the resulting $k$ parameters; b) the calculated diameter of confined water during the pore-filling process (Eq. (6)), where the dashed lines show the filled state; c) the $T_2$ relaxation distributions from the inverse-Laplace transformation at the filled state ($f = 1$) and d) the derived pore size distributions calculated with Eq. (6). (A colour version of this figure can be viewed online.)

between the measured relaxation time and the filling factor in partially filled systems [64]:

$$T_2 \cong T_{2s}\frac{V_p}{lS_p}f^k \tag{5}$$

Fig. 7a shows this type of representation for our data. Fitting of Eq. (5) to the measured $T_2$ data can quantify the wetting mechanism according to Ardelean's concept of the kinetic term, $k$. In Eq. (5) $k$ is zero in the case of exclusively plug-like saturation, while $k = 1$ when the loading is uniform (explained in details in the SI). The $k$ values between 0 and 1 indicate an intermediate process resulting in a nonlinear function of $T_2$ on $f$ [37,38].

The fitting of our experimental data, shown in Fig. 7a, gave $k = 0.23$ (±0.03) and $k = 0.6$ (±0.08) for CA1 and CA2 respectively. These results show that only a certain part of the water layer on the surface contributes to the exchange process with the bulk-like water molecules, meaning that the water distribution is not completely uniform on the pore surface of both aerogels. This observation is in line with previous results on carbon materials [28,29], and indicates that after a certain amount of added water pores fill one after one another as we concluded from the cryoporometric experiments. Furthermore, the higher $k$ value of CA2 means that more surface water is in contact with the pore water, that is the wetting is more uniform in character than in the case of CA1. It can be the result of the different surface properties of CA2, which was already shown by the measured constantly low relaxation times ($T_{2a}$ in Fig. 6b).

There is one point neglected in the above arguments: there can be exchange between the surface water and the bulk-like water by vapor diffusion, which is much faster than the bulk diffusion. It gives rise to the exchange process between waters which are not in direct contact, thus might yield a higher $k$ value, featuring a more uniform character to the wetting mechanism. In case of hydrophobic pore walls this is a rational assumption, that is our $k$ value is over-estimated, which strengthens the "plug-like" saturation model.

From cryoporometry it is known that the pores filled with water show spherical geometry, thus the $S_p/V_p$ can be replaced by $3/r$ in equation (5), resulting in Eq. (6).

$$T_2 \cong T_{2s}\frac{r}{3l}f^k \tag{6}$$

This means that the fitting procedure in Fig. 7a can be used to determine the thickness of the surface water layer ($l$). For this calculation the pore radii are known from cryoporometry ($r = 21$ and 25 nm for CA1 and CA2, respectively) and $T_{2s}$ is measured (5.3 ms for CA1, while 1.6 ms, an averaged value for CA2). The results are presented in Table 2. The thickness of the surface water layer ($l$) is practically equal for both aerogels (~0.2 nm) meaning experimental evidence for the similar sized water clusters of carbon aerogels, prepared in a different way. For different carbon nanomaterials $l$ values between 0.2 and 0.3 nm were estimated in the literature which are comparable with our results [25,34].

The difference in the hydrophilic/hydrophobic properties is

reflected in the surface relaxation strength ($\xi$), which can be derived from Eq. (4) using the determined $l$ values (as $l/T_{2s}$). It means that the effect of pore surface on confined water is expressed by the surface relaxation time ($T_{2s}$) and the effective range of the interaction between the surface and the attached water ($l$). They have the same effect on the surface relaxivity ($\xi$) of the system, thus it is usually very difficult to separate them (Eq. (4)). Table 2 shows that $\xi$ is higher for CA2 by one order of magnitude, meaning a stronger relaxation effect of the surface on the bound water clusters. This is responsible for the generally shorter relaxation times measured in CA2 as well. The determined $\xi$ values are higher, than that calculated by Bardenhagen et al. [27] for carbon xerogels, which can be related to the different synthesis and character of the studied materials.

Using Eq. S(6) the radii of the spherical pores can be expressed and calculated from the transverse relaxation times as well. In Fig. 7b these data are presented in diameter ($d = 2r$) during the pore-filling process (up to $f = 1$), showing approximately 45–50 nm pore size in the filled state (dashed lines in Fig. 7b), confirming that there is no inconsistency in our arguments. As mentioned above we evaluated the exponential relaxation decays with inverse-Laplace transformation, resulting in $T_2$ relaxation distribution curves at $f = 1$ shown in Fig. 7c. These $T_2$ distributions were inverted into pore size distribution curves (Fig. 7d), which is in good agreement with the cryoporometry (Fig. 5d) even if the two methods have different basics.

### 3.2.4. Self-diffusion and distribution of water in the pore structure

Water diffusion in the pore system was investigated by NMR diffusometry at several partially filled states up to the oversaturation of both carbon aerogels. The diffusion coefficients of water were derived from Eq. (7).

$$I = \sum_{i=1}^{n} I_{0i} \exp\left( - D_{obs,i} \gamma^2 \delta^2 G^2 (\Delta - \delta / 3) \right) , \qquad (7)$$

where $I$ is the measured signal intensity, $I_{0i}$ are the initial intensities in the separated spin reservoirs, $D_{obs,i}$ is the apparent diffusion coefficient, $\gamma$ is the gyromagnetic ratio of the given nucleus, $\delta$ is the duration of the gradient pulse, $G$ is the gradient strength, while $\Delta$ is the diffusion time.

As mentioned above (see the morphology section) the high-resolution $^1$H NMR spectra of water in the aerogels show two peaks; the peak of pore-filling water and that of the water clusters,separately with changing intensity ratio (see Fig. 4) at water contents up to 2.4 and 0.2 g/g for CA1 and CA2, respectively. Diffusion measurements and data evaluations were performed for both peaks as long as they were observable. There were two surprising results: both peaks could be described with two independent apparent diffusion coefficients (in Eq. (7) $n = 2$), and one of them was higher, while the other was lower than that of the bulk water. The two-dimensional DOSY spectrum in Fig. 8 demonstrates well the presence of these four diffusion coefficients. The lower $D_{obs}$ values are very common in porous media, they result from the restricted liquid diffusion (indicating filled or dominantly filled pores) and are discussed in details in the literature [65]. The higher diffusivity is dominated by diffusion in vapor phase in partially filled pores; as it can be rarely detected, a thorough justification is given in the SI [42]. For an evidence of vapor phase effect when cooling sample CA1 with 5.69 g/g water content, the diffusion contribution of the vapor phase became negligible as a result of the lower vapor pressure [42]. The calculated diffusion coefficients at every measured filling state are presented in Fig. 9a and b.

Above such high water contents where the influence of the vapor phase becomes negligible, the error of the biexponential fitting increases, and only one peak with a single exponential decay is observed with a diffusion coefficient close to that of bulk water. It is consistent with the results of cryoporometry: when the spherical pores are saturated (4.8 g/g and 1.16 g/g water content for CA1 and CA2), the continuous filling up of the connecting channels takes place, thus the role of vapor diffusion decreases, only the liquid diffusion is operative (Fig. 9). This is also confirmed by Fig. 9c and d, showing that the vapor-dominated diffusion domains gradually disappear with increasing water content, and the pores fill up completely.

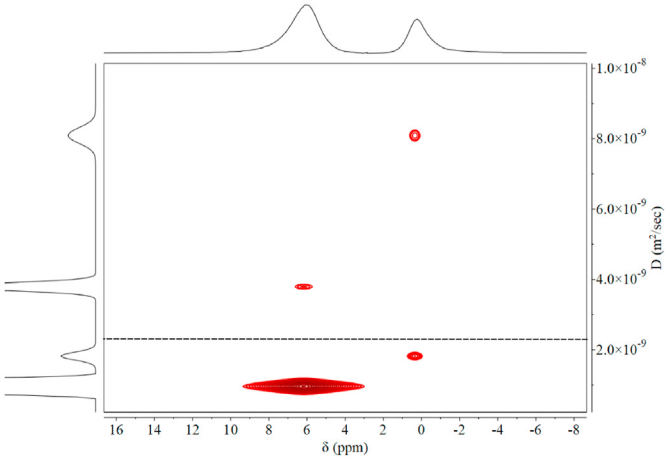


**Fig. 8.** Two-dimensional DOSY spectrum of CA1 sample at 0.98 g/g water content. The dashed line stands for the diffusion coefficient of bulk water ($2.3 \times 10^{-9}$ m$^2$/s) [55]. (A colour version of this figure can be viewed online.)

This description is very characteristic for the more hydrophobic CA1 while less conspicuous for CA2 supporting our statement above about its more hydrophilic character. The distribution of these four water sites indicated with 1–4 is illustrated in Fig. 10 and explained for CA1 as follows.

Water in the mesopores, attributed to the peak at 7 ppm chemical shift, shows two states (Fig. 10):

(1) *Filled mesopores*: The slow diffusion component is the restricted diffusion of liquid water in the completely filled mesopores. It is constant until 4.5 g/g filling, being between 1.1 and $1.3\times10^{-9}$ m$^2$ s$^{-1}$, then slowly increases and almost reaches the diffusion rate of free water. This domain involves the highest water amount, which increases during the saturation as Fig. 9c confirms.

(2) *Partially filled mesopores*: The vapor diffusion is dominant in this domain. $D$ is around $5 \times 10^{-9}$ m$^2$s$^{-1}$, which slightly decreases with the water content and becomes not observable above 6 g/g concentration. Although we have a few evidences showing that the spherical pores fill up after each other, there can still be some partially filled pores where in the average the vapor diffusion is dominant, being faster than the water diffusion in the bulk solvent. Fig. 9c shows that only about 20% of the spherical pores are partially filled during the saturation.

The ratio of filled (1) and partially filled (2) pores is only slightly changing during the saturation (about 80% and 20% respectively), and their collective contribution increases (Fig. 9c). This result is in accordance with the cryoporometric and relaxometric results, namely that the pores saturate one after another, with an identical mechanism, and the water distribution is non-uniform. The carbon

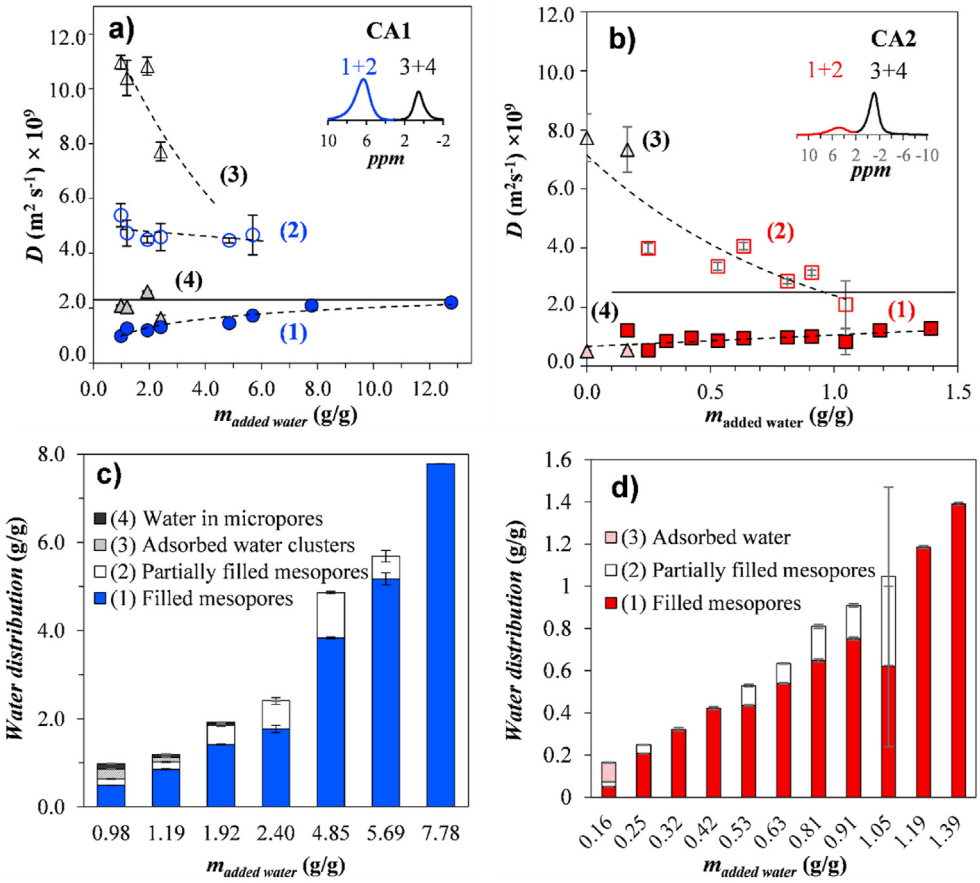


**Fig. 9.** a-b) Diffusion coefficients of water in RF carbon aerogels as a function of the water content at 298 K. Empty and filled symbols stand for the diffusion coefficients dominated by vapor and restricted diffusion respectively, corresponding in color to the $^1$H NMR spectrum (inset, at the lowest water contents). The solid line displays the theoretical value for bulk water ($2.3\times10^{-9}$ $m^2s^{-1}$) [55] as a reference, while dashed lines are only a guide to the eyes. The error bars were derived from the standard deviation of *D* obtained from the exponential fitting. c-d) The distribution of water among the water domains at increasing water content, calculated from the peak integrals and amplitudes of the biexponential fittings for CA1 and CA2, respectively. (A colour version of this figure can be viewed online.)

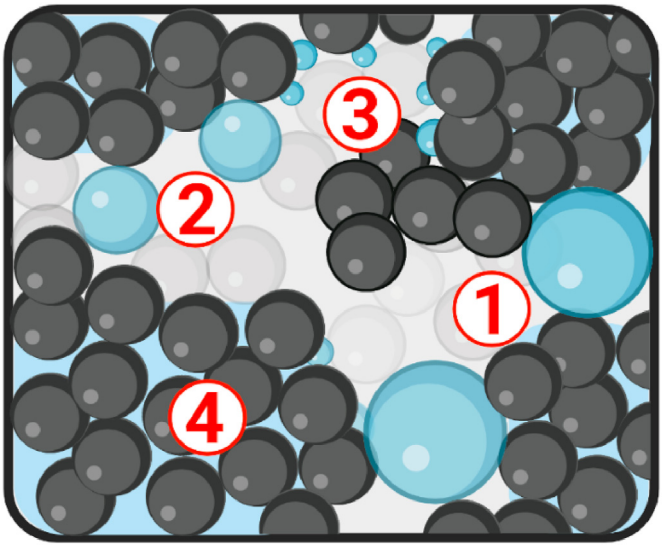


**Fig. 10.** Water domains in the partially filled pore structure of the carbon aerogels. Black spheres stand for the carbon aerogel skeleton, while blue color shows the water in the pore system. Numbers indicate the different diffusion domains of water as numbered in the text. (A colour version of this figure can be viewed online.)

aerogel behaves macroscopically at these water contents like dry powder. It means that after mixing there are mostly completely filled islands of mesopores and some partially filled pores. There is no water exchange connection between them therefore two-step diffusion can be measured.

Water clusters, represented by the peak at 0.5 ppm chemical shift and observed at low water contents, can be subdivided into two types as well:

(3) *Water clusters around the hydrophilic functional groups in the empty meso- and macropores*: The liquid is in connection with large vapor-filled pores therefore the diffusion is dominated by vapor diffusion. The measured large diffusion coefficient ($D \approx$ 1.1-1.2 $\times$ $10^{-8}$ $m^2s^{-1}$) is an average, weighted by the volume ratio of water diffusing in the liquid and air phases. It is difficult to make quantitative estimation either on the liquid component or the vapor component because of the tortuosity of the pores and the unknown surface mobility of water [42].

(4) *Water in micropores*: In this other type of bound water the diffusion takes place in the liquid phase dominantly, but is influenced by the vapor phase as well, thus we suppose that these molecules are located in the filled micropores connected to empty meso- and macropores. Because of the small air space and small liquid surface in connection with them, the measured diffusion coefficient is dominated by the

restricted diffusion of water in the liquid state, but the relatively high averaged $D$ value, being close to bulk water ($D = 2.3\times10^{-9}$ $m^2s^{-1}$, [55]) still shows a non-negligible contribution of vapor diffusion. The relatively constant diffusion coefficients until 2.4 g/g water indicate that this water domain is already saturated, as deduced also from relaxometry, and this water does not freeze at the lowest temperature applied in cryoporometry.

Both domains have less and less contribution during the pore filling process as Fig. 9c shows, and get negligible above 2.4 g/g water content.

In the case of CA2 the $^1$H NMR peak assigned to the adsorbed water clusters can be detected only in the air-dried sample and at the first water addition step (Fig. 4). At higher water contents one broad water peak can be observed with a biexponential diffusion decay. The two diffusion domains determined were related to (1) and (2) states of water, i.e., water molecules filling the spherical mesopores, as explained above. This is confirmed by the similar values and trends of the data, and the melting and freezing processes measured by NMR cryoporometry. According to $N_2$ gas adsorption the micropore volume of CA2 is lower than that of CA1, NMR relaxometry shows a low amount of water clusters on the surface, which explain the disappearance of the (3) and (4) water domains.

### 3.3. Comparison of the carbon aerogels

Owing to the different porogens applied in the synthesis the two carbon samples possess considerably different pore morphology. The dissimilarity of the pore morphology is the most expressed in the mesopore range. The surface area, the total pore volume and the volumes of all the pore categories detected with nitrogen adsorption are significantly higher in the CA1 carbon aerogel. On the other hand, the morphology of CA1 and CA2 is also similar in several aspects. Their structure is built of 20 nm carbon beads, separated with interconnected micro-, meso- and macropores. Based on the nitrogen adsorption results the most typical size of the mesopores varies from 3 to 27 nm and the typical size of the entrance of the mesopores is 20 nm. Based on the NMR measurements using water as probe solvent the presence of 40–50 nm spherical pores are detected.

A remarkable difference is observed in the pore texture during the wetting process. It starts in the same way for both aerogels, as the water vapor adsorption isotherms revealed. Water is adsorbed on the hydrophilic functional groups of the carbon skeleton, forms water clusters, and fills the micropores, according to the mechanism generally described in the literature [13].

However, NMR relaxometry results have shown, that the wetting properties of the mesopores in the studied carbon aerogels differ. In the case of CA2 the measured $T_2$ relaxation times are significantly lower, than for CA1, which indicates a stronger effect of the surface on the entrapped water molecules. As it was mentioned in the previous sections, the filling of the micropores and the pore sizes are basically similar, thus they cannot be the reason for the lower $T_2$. Another explanation could lie in the surface properties although, XPS and water vapor adsorption didn't show differences between CA1 and CA2. The detailed evaluation of relaxometry results revealed that the surface water layer thickness ($l$) is approximately the same for both aerogels, thus the surface relaxivity ($\xi$) should be different. The significantly higher surface relaxivity of CA2 can only be explained by the higher density of hydrophilic functional groups, their better accessibility or higher affinity to water molecules. The wetting process of the mesopores in the carbon aerogels according to these NMR results is demonstrated in Fig. 11.

The above sorted differences are visible in the behavior of the two samples during the immersion as well. CA1 was powder-like at high water contents, while CA2 seized even at a much lower filling state. The wetting of the porous structure is plug-like, especially for CA1, i.e., the water distribution is non-uniform and pores get filled with water one after another. During the saturation process, vapor diffusion was observed in the partially filled structure up to the complete filling of the spherical pores in both materials. The combined use of the applied techniques revealed the differences in the porous texture caused by the different media during the synthesis.

## 4. Conclusions

Application of various NMR methods combined with sorption techniques can reveal such differences between porous materials which remain hidden at separate use of the techniques. The first step of the characterization should be the $N_2$ gas adsorption method which gives information about the dry structure of the synthesized aerogels. XPS describes the chemical composition of the surface while water vapor adsorption, beyond the surface chemistry, points at the behavior in wet state, that is under the circumstances of possible applications.

The combined use of NMR relaxometry, diffusiometry and

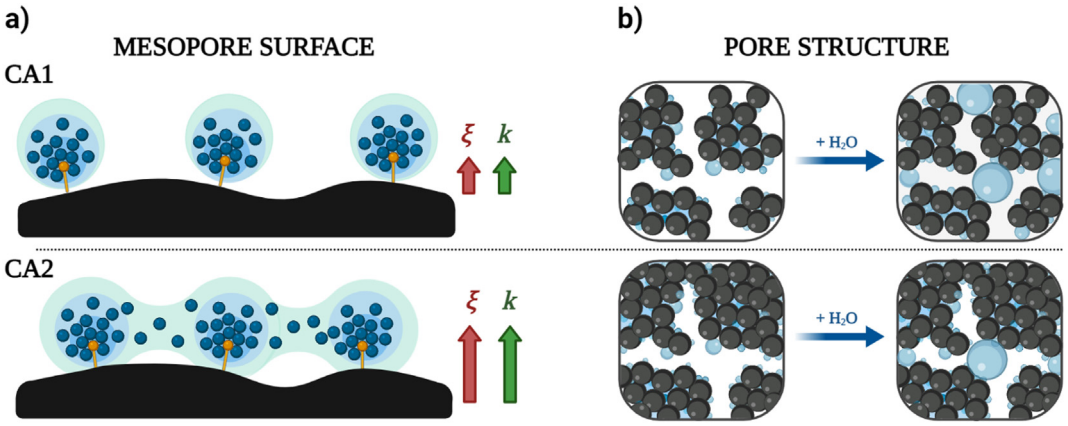


**Fig. 11.** Wetting process of the mesopores of CA1 and CA2 carbon aerogels as seen by NMR a) on the pore surface and b) in the pore system. The carbon aerogel skeleton is signed with black color, the functional groups are yellow, while blue color shows the water in the pore system. (A colour version of this figure can be viewed online.)

cryoporometry is able to provide a complex description and model of the hydration and pore filling mechanism of carbon-based materials up to the oversaturated state. In this study the wetting process of two carbon aerogels, synthesized in different way, was followed. The three NMR methods proved that due to the partially hydrophobic surface, the filling of the meso- and macropores takes place separately, *i.e.,* the distribution of water in the pore system is non-uniform, but in different extent for the two aerogel samples. The complete saturation of the mesopores could be detected by all the three NMR methods providing new tools to reach this important information.

With the comparison of the NMR and sorption methods, information was gained on the hydrophilic/hydrophobic properties of the pore surface as well as the different macroscopic appearance of the samples under wetting. Furthermore, they can predict the affinity of these carbon aerogels toward polar/nonpolar adsorbates and their behavior in aqueous medium for numerous possible applications, like industrial catalysts and environmental adsorbents.

## CRediT authorship contribution statement

**Mónika Kéri:** Data curation, Writing – original draft, Investigation. **Dávid Nyul:** Writing – original draft, Investigation. **Krisztina László:** Data curation, Writing – original draft. **Levente Novák:** Writing – review & editing. **István Bányai:** Conceptualization, Project administration.

## Declaration of competing interest

The authors declare that they have no known competing financial interests or personal relationships that could have appeared to influence the work reported in this paper.

## Acknowledgement

The research has been implemented with the support provided from the National Research, Development and Innovation Office of Hungary, financed under the NKFIH K_131989 funding scheme. Mónika Kéri is grateful for the National Research, Development and Innovation Office of Hungary (NKFIH: PD_135169) for financial support. The research was also supported by the EU and co-financed by the European Regional Development Fund under the project GINOP-2.3.2-15-2016-00008. Financial support of VEKOP-2.3.2-16-2017-00013 (supported by the EU and by Hungary, co-financed by the European Regional Development Fund) is acknowledged. The work is also part of the EU project NANOMED (H2020-MSCA-RISE-2016, #734641). We are grateful to Balázs Nagy for the aerogel synthesis.

## Appendix A. Supplementary data

Supplementary data to this article can be found online at https://doi.org/10.1016/j.carbon.2021.12.045.

## References

[1] E. Frackowiak, F. Béguin, Carbon materials for the electrochemical storage of energy in capacitors, Carbon 39 (6) (2001) 937–950.
[2] C. Moreno-Castilla, F.J. Maldonado-Hódar, Carbon aerogels for catalysis applications: an overview, Carbon 43 (3) (2005) 455–465.
[3] L.W. Hrubesh, Aerogel applications, J. Non-Cryst. Solids 225 (1998) 335–342.
[4] Y. Zhu, H. Hu, W. Li, X. Zhang, Resorcinol-formaldehyde based porous carbon as an electrode material for supercapacitors, Carbon 45 (1) (2007) 160–165.
[5] A.M. ElKhatat, S.A. Al-Muhtaseb, Advances in tailoring resorcinol-formaldehyde organic and carbon gels, Adv. Mater. 23 (26) (2011) 2887–2903.
[6] B. Nagy, Tailored Carbon Aerogels and Their Possible Applications, Faculty Of Chemical Technology And Biotechnology, George Oláh Phd School, Budapest University Of Technology And Economics, Budapest, 2017.
[7] B. Nagy, I. Bakos, E. Geissler, K. László, Water-ionic liquid binary mixture tailored resorcinol-formaldehyde carbon aerogels without added catalyst, Materials (Basel) 12 (24) (2019) 4208.
[8] A. Allahbakhsh, A.R. Bahramian, Self-assembled and pyrolyzed carbon aerogels: an overview of their preparation mechanisms, properties and applications, Nanoscale 7 (34) (2015) 14139–14158.
[9] S.A. Al-Muhtaseb, J.A. Ritter, Preparation and properties of resorcinol-formaldehyde organic and carbon gels, Adv. Mater. 15 (2) (2003) 101–114.
[10] N. Hebalkar, G. Arabale, S.R. Sainkar, S.D. Pradhan, I.S. Mulla, K. Vijayamohanan, P. Ayyub, S.K. Kulkarni, Study of correlation of structural and surface properties with electrochemical behaviour in carbon aerogels, J. Mater. Sci. 40 (14) (2005) 3777–3782.
[11] A. Tóth, K. László, Chapter 5 - water adsorption by carbons. Hydrophobicity and hydrophilicity, in: J.M.D. Tascón (Ed.), Novel Carbon Adsorbents, Elsevier, Oxford, 2012, pp. 147–171.
[12] R. Kleinberg, Nuclear magnetic resonance, in: R. Celotta, T. Lucatorto (Eds.), Methods in the Physiscs of Porous Media, Academic Press1999, pp. 337-385.
[13] L. Liu, S. Tan, T. Horikawa, D.D. Do, D. Nicholson, J. Liu, Water adsorption on carbon - a review, Adv. Colloid Interfac. 250 (2017) 64–78.
[14] V.M. Gun'ko, V.V. Turov, Nuclear Magnetic Resonance Studies of Interfacial Phenomena, CRC Press, NewYork, 2013, pp. 455–522.
[15] D.T. Shane, R.L. Corey, C. McIntosh, L.H. Rayhel, R.C. Bowman, J.J. Vajo, A.F. Gross, M.S. Conradi, LiBH4 in carbon aerogel nanoscaffolds: an NMR study of atomic motions, J. Phys. Chem. C 114 (9) (2010) 4008–4014.
[16] F. D Orazio, S. Bhattcharja, J.C. Tarczon, W.P. Halperin, Magnetic resonance relaxation analyísis of porous media, in: J. Klafter, J.M. Draker (Eds.), Molecular Dynamics in Resricted Geometries, Wiley, New York, 1989.
[17] P.J. Barrie, Characterization of porous media using NMR methods, Annu. Rep. NMR Spectrosc. 41 (2000) 265–316.
[18] O.V. Petrov, I. Furó, Curvature-dependent metastability of the solid phase and the freezing-melting hysteresis in pores, Phys. Rev. E 73 (2006), 011608.
[19] O.V. Petrov, I. Furó, NMR cryoporometry: principles, applications and potential, Prog. Nucl. Magn. Reson. Spectrosc. 54 (2) (2009) 97–122.
[20] O. Petrov, I. Furó, A study of freezing–melting hysteresis of water in different porous materials. Part II: surfactant-templated silicas, Phys. Chem. Chem. Phys. 13 (36) (2011) 16358–16365.
[21] O. Petrov, I. Furó, A study of freezing–melting hysteresis of water in different porous materials. Part I: porous silica glasses, Microporous Mesoporous Mater. 138 (1) (2011) 221–227.
[22] M. Kéri, A. Forgács, V. Papp, I. Bányai, P. Veres, A. Len, Z. Dudás, I. Fábián, J. Kalmár, Gelatin content governs hydration induced structural changes in silica-gelatin hybrid aerogels - implications in drug delivery, Acta Biomater. 105 (2020) 131–145.
[23] D. Fairhurst, T. Cosgrove, S.W. Prescott, Relaxation NMR as a tool to study the dispersion and formulation behavior of nanostructured carbon materials, Magn. Reson. Chem. 54 (6) (2016) 521–526.
[24] G.S. Gogelashvili, R.S. Vartapetyan, D.V. Ladychuk, Y.B. Grunin, E.V. Khozina, Specific features of the adsorption and nuclear magnetic relaxation of water molecules in active carbons. 1. Relation between the spin-spin relaxation of adsorbed water molecules and structural parameters of microporous active carbons, Colloid J. Russ. Acad+ 65 (5) (2003) 545–551.
[25] G.S. Gogelashvili, R.S. Vartapetyan, D.V. Ladychuk, Y.B. Grunin, E.V. Khozina, Specific features of the adsorption and nuclear magnetic relaxation of the water molecules in active carbons: 2. The state of water in active carbon with relatively large pores according to the NMR relaxation data, Colloid J. 66 (3) (2004) 271–276.
[26] H.-J. Wang, A. Kleinhammes, T.P. McNicholas, J. Liu, Y. Wu, Water adsorption in nanoporous carbon characterized by in situ NMR: measurements of pore size and pore size distribution, J. Phys. Chem. C 118 (16) (2014) 8474–8480.
[27] I. Bardenhagen, W. Dreher, D. Fenske, A. Wittstock, M. Bäumer, Fluid distribution and pore wettability of monolithic carbon xerogels measured by 1H NMR relaxation, Carbon 68 (2014) 542–552.
[28] C. Cadar, C. Cotet, L. Baia, I. Ardelean, Probing the connectivity and wettability of carbon aerogels and xerogels via low-field NMR, AIP Conf. Proc. 1917 (1) (2017), 040006.
[29] C. Cadar, C. Cotet, L. Baia, L. Barbu-Tudoran, I. Ardelean, Probing into the mesoporous structure of carbon xerogels via the low-field NMR relaxometry of water and cyclohexane molecules, Microporous Mesoporous Mater. 251 (2017) 19–25.
[30] I. Yu, M. Lee, 1H NMR study of water adsorbed on carbon powders, J. Magn. Reson., Ser. A 109 (1) (1994) 41–45.
[31] X. Liu, X. Pan, S. Zhang, X. Han, X. Bao, Diffusion of water inside carbon nanotubes studied by pulsed field gradient NMR spectroscopy, Langmuir 30 (27) (2014) 8036–8045.
[32] Y. Zhao, Y. Sun, S. Liu, K. Wang, Y. Jiang, Pore structure characterization of coal by NMR cryoporometry, Fuel 190 (2017) 359–369.
[33] M. Keri, B. Nagy, K. László, I. Bányai, Structural changes in resorcinol formaldehyde aerogel seen by NMR, Microporous Mesoporous Mater. 317 (2021) 110988.
[34] S. Ghosh, K.V. Ramanathan, A.K. Sood, Water at nanoscale confined in single-walled carbon nanotubes studied by NMR, Europhys. Lett. 65 (5) (2004) 678.
[35] M. Krutyeva, F. Grinberg, F. Furtado, P. Galvosas, J. Karger, A. Silvestre-Albero, A. Sepulveda-Escribano, J. Silvestre-Alberto, F. Rodriguez-Reinoso,

Characterization of carbon materials with the help of NMR methods, Microporous Mesoporous Mater. 120 (1–2) (2009) 91–97.
[36] S.G. Allen, P.C.L. Stephenson, J.H. Strange, Morphology of porous media studied by nuclear magnetic resonance, J. Chem. Phys. 106 (18) (1997) 7802–7809.
[37] A. Bede, A. Scurtu, I. Ardelean, NMR relaxation of molecules confined inside the cement paste pores under partially saturated conditions, Cement Concr. Res. 89 (2016) 56–62.
[38] M. Simina, R. Nechifor, I. Ardelean, Saturation-dependent nuclear magnetic resonance relaxation of fluids confined inside porous media with micrometer-sized pores, Magn. Reson. Chem. 49 (6) (2011) 314–319.
[39] S.G. Allen, P.C.L. Stephenson, J.H. Strange, Internal surfaces of porous media studied by nuclear magnetic resonance cryoporometry, J. Chem. Phys. 108 (19) (1998) 8195–8198.
[40] I. Ardelean, G. Farrher, C. Mattea, R. Kimmich, NMR study of the vapor phase contribution to diffusion in partially filled silica glasses with nanometer and micrometer pores, Magn. Reson. Imaging 23 (2) (2005) 285–289.
[41] I. Ardelean, G. Farrher, C. Mattea, R. Kimmich, Nuclear magnetic resonance study of the vapor contribution to diffusion in silica glasses with micrometer pores partially filled with liquid cyclohexane or water, J. Chem. Phys. 120 (20) (2004) 9809–9816.
[42] F. D'Orazio, S. Bhattacharja, W.P. Halperin, R. Gerhardt, Enhanced self-diffusion of water in restricted geometry, Phys. Rev. Lett. 63 (1) (1989) 43–46.
[43] F. D'Orazio, S. Bhattacharja, W.P. Halperin, R. Gerhardt, Fluid transport in partially filled porous sol-gel silica glass, Phys. Rev. B 42 (10) (1990) 6503–6508.
[44] S. Brunauer, P.H. Emmett, E. Teller, Adsorption of gases in multimolecular layers, J. Am. Chem. Soc. 60 (2) (1938) 309–319.
[45] M.M. Dubinin, L.V. Radushkevich, The Equation of the Characteristic Curve of Activated Charcoal, Chem. Zentr., 1947, pp. 875–890.
[46] E.P. Barrett, L.G. Joyner, P.P. Halenda, The determination of pore volume and area distributions in porous substances. I. Computations from nitrogen isotherms, J. Am. Chem. Soc. 73 (1) (1951) 373–380.
[47] H.Y. Carr, E.M. Purcell, Effects of diffusion on free precession in nuclear magnetic resonance experiments, Phys. Rev. 94 (3) (1954) 630–638.
[48] S. Meiboom, D. Gill, Modified spin-echo method for measuring nuclear relaxation times, Rev. Sci. Instrum. 29 (8) (1958) 688–691.
[49] C. Ammann, P. Meier, A. Merbach, A simple multinuclear NMR thermometer, J. Magn. Reson. 46 (2) (1982) 319–321, 1969.
[50] D. Kehl, B. Sipos, A telítődési, a logisztikus és az életgörbe alakú trend-függvények becslése Excel parancsfájl segítségével, Statisztikai Szle. 87 (4) (2009) 381–411 (in Hungarian).
[51] D.A. Reiter, P.-C. Lin, K.W. Fishbein, R.G. Spencer, Multicomponent T2 relaxation analysis in cartilage, Magn. Reson. Med. 61 (2009) 803–809.
[52] S. Godefroy, P.T. Callaghan, 2D relaxation/diffusion correlations in porous media, Magn. Reson. Imaging 21 (3) (2003) 381–383.
[53] M.D. Does, M.R. Juttukonda, R.D. Dortch, MERA Toolbox (1D,2D Multi-Exponential Relaxation Analysis), Vanderbilt University.
[54] C.S. Johnson, Diffusion ordered nuclear magnetic resonance spectroscopy: principles and applications, Prog. Nucl. Magn. Reson. Spectrosc. 34 (3) (1999) 203–256.
[55] R. Mills, Self-diffusion in normal and heavy water in the range 1-45.deg, J. Phys. Chem. 77 (5) (1973) 685–688.
[56] H. Kato, T. Saito, M. Nabeshima, K. Shimada, S. Kinugasa, Assessment of diffusion coefficients of general solvents by PFG-NMR: investigation of the sources error, J. Magn. Reson. 180 (2) (2006) 266–273.
[57] M. Thommes, K. Kaneko, V. Neimark Alexander, P. Olivier James, F. Rodriguez-Reinoso, J. Rouquerol, S.W. Sing Kenneth, Physisorption of gases, with special reference to the evaluation of surface area and pore size distribution (IUPAC Technical Report), Pure Appl. Chem. (2015) 1051.
[58] K.A. Cychosz, R. Guillet-Nicolas, J. García-Martínez, M. Thommes, Recent advances in the textural characterization of hierarchically structured nanoporous materials, Chem. Soc. Rev. 46 (2) (2017) 389–414.
[59] B. Nagy, S. Villar-Rodil, J.M.D. Tascón, I. Bakos, K. László, Nitrogen doped mesoporous carbon aerogels and implications for electrocatalytic oxygen reduction reactions, Microporous Mesoporous Mater. 230 (2016) 135–144.
[60] E.A. Müller, L.F. Rull, L.F. Vega, K.E. Gubbins, Adsorption of water on activated carbons:A molecular simulation study, J. Phys. Chem. 100 (4) (1996) 1189–1196.
[61] K. Kaneko, Y. Hanzawa, T. Iiyama, T. Kanda, T. Suzuki, Cluster-mediated water adsorption on carbon nanopores, Adsorption 5 (1) (1999) 7–13.
[62] V.M. Gun'ko, V.V. Turov, O.P. Kozynchenko, D. Palijczuk, R. Szmigielski, S.V. Kerus, M.V. Borysenko, E.M. Pakhlov, P.P. Gorbik, Characteristics of adsorption phase with water/organic mixtures at a surface of activated carbons possessing intraparticle and textural porosities, Appl. Surf. Sci. 254 (10) (2008) 3220–3231.
[63] B. Nagy, A. Tóth, I. Savina, S. Mikhalovsky, L. Mikhalovska, E. Geissler, K. László, Double probe approach to protein adsorption on porous carbon surfaces, Carbon 112 (2017) 103–110.
[64] F. Gallego-Gómez, C. Cadar, C. López, I. Ardelean, Imbibition and dewetting of silica colloidal crystals: an NMR relaxometry study, J. Colloid Interface Sci. 561 (2020) 741–748.
[65] W.S. Price, Pulsed-field gradient nuclear magnetic resonance as a tool for studying translational diffusion: Part 1. Basic theory, Concepts Magn. Reson. 9 (5) (1997) 299–336.